Project Title: Low-Temperature, Anode-Supported High Power Density Solid Oxide Fuel Cells with Nanostructured Electrodes

Quarterly Technical Report

October 1, 1999 – March 31, 2000

Contract Number: DE-AC26-99FT40713

Principal Investigator: Prof. Anil V. Virkar
Department of Materials Science & Engineering
122 S. Central Campus Drive
University of Utah
Salt Lake City, UT 84112
Phone: (801) 581-5396
Fax: (801) 581-4816
Email: anil.virkar@m.cc.utah.edu

Submitted: April 7, 2000

Disclaimer:

This report contains the following three parts.

1) An investigation into the use of direct liquid hydrocarbon fuels in single cell tests.
2) An analysis of residual stresses in anode-supported solid oxide fuel cells.
3) A manuscript on the synthesis of nanosize ceramic (electrode and electrolyte) powders.

A Single Cell Test on Ethanol + Water as a Fuel: One of the potential benefits of anode-supported solid oxide fuel cells (SOFC) is the possibility of using hydrocarbon fuels directly without the necessity of external reforming. High performance fuel cells with a low overall area specific resistance (ASR), achieved through appropriate electrode microstructural design, should facilitate this at relatively lower temperatures. Anode-supported single cells comprising a porous Ni + YSZ (yttria-stabilized zirconia) as the anode, a thin dense film of YSZ as the electrolyte, and a porous Sr-doped $LaMnO_3$ (LSM) + YSZ as the cathode were fabricated by tape-casting of NiO +YSZ anode precursor, spray-coating YSZ electrolyte, sintering, and applying the cathode. A solution of ethanol (C_2H_5OH) in water in 1:2 proportion was made. This liquid was vaporized and introduced into the anode chamber. The cell was operated at 800^{o}C. Figure #1 shows the performance characteristics of the cell. As can be seen, power densities as high as 0.8 W/cm^2 were observed wherein the fuel was internally reformed. The anode of the cell has not been yet designed for use with hydrocarbon fuels. It is anticipated that once this is achieved, even higher power densities should be possible. No carbon deposition was observed.

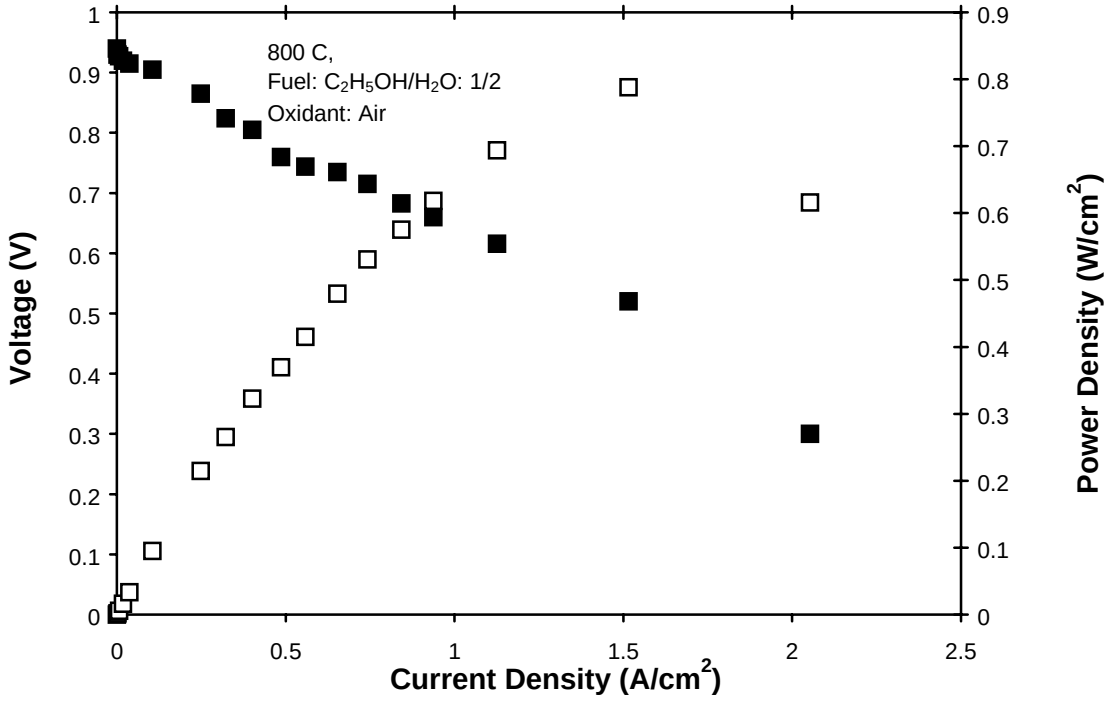

Figure #1: Voltage and power density vs. current density of a single cell tested with ethanol + water as the fuel and air as the oxidant, at 800^{o}C.

Residual Stresses in Anode-Supported Cells: In anode-supported cells with Ni + YSZ as the anode and YSZ as the electrolyte, at low temperature, the YSZ thin film is in a state of biaxial compression. This is because the coefficient of thermal expansion of YSZ is lower than that of Ni. Since the film is expected to be in compression, it is no expected to crack. However, if the film is too thick, there is the potential that it can delaminate or spall off. The propensity for delamination is higher at low temperatures, not at the operating temperature. However, it is necessary that the film be well-adherent at room temperature since the SOFC will be typically cycled between room temperature and the operating temperature. An effort to evaluate the state of stress using finite element technique has been initiated. Preliminary results are presented in what follows.

Finite Element Analysis of Film and Substrate

Finite element analysis of following film (YSZ electrolyte) - substrate (Ni + YSZ anode) was performed by using ANSYS 5.5 (Finite Element Analysis package). The analysis is steady state structural analysis and the element used is PLANE42.
Following parameters were used in the analysis:
α_1 = Coefficient of thermal expansion of the film. =10.5 x 10^{-6} /^{o}C
α_2 = Coefficient of thermal expansion for substrate. =13 x 10^{-6}/°C
E_1 = Young's modules of elasticity for film = 210 GPa
E_2 = Modules of Elasticity for substrate. = 170 GPa
$\Delta\varepsilon = \Delta\alpha\Delta T$=3.25 x 10^{-3}

Coordinate System:

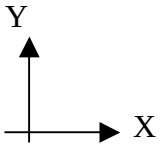

Figure 1:

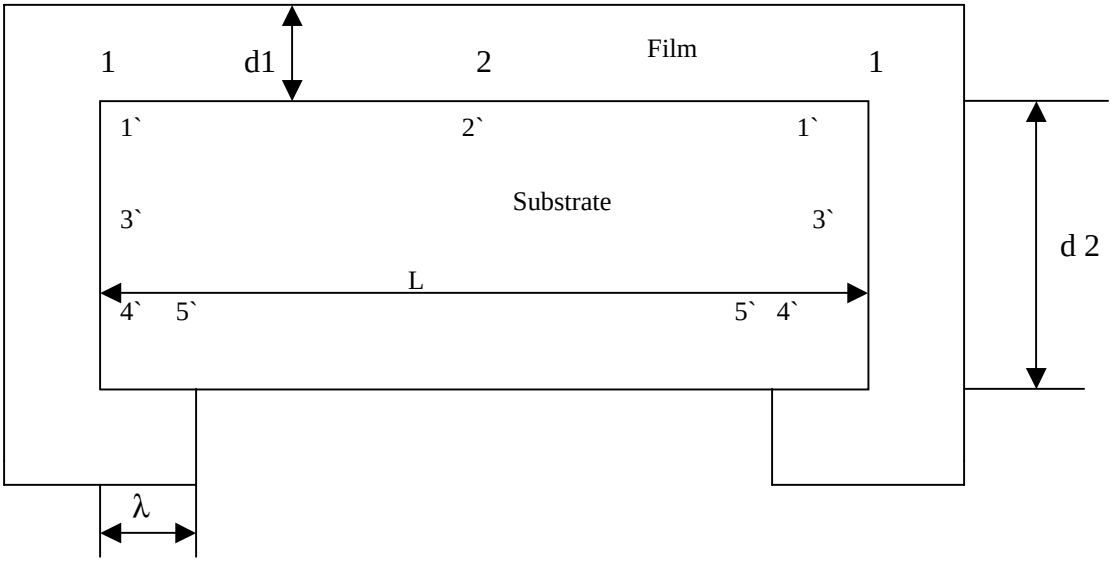

λ = 5 mm, d_1 = 0.025 mm, d_2 = 1.5 mm, L = 50 mm.

Location	Sxx(MPa)	Syy(MPa)	Location	Sxx(MPa)	Syy(MPa)
1	-207.98	-409.00	1`	59.085	56.458
2	-606.37	-0.43E-03	2`	61.627	-0.88E-03
3	-0.788	-656.58	3`	-1.026	61.383
4	-431.04	-172.26	4`	60.205	65.515
5	-620.73	8.781	5`	-0.57E-01	2.73

Figure 2:

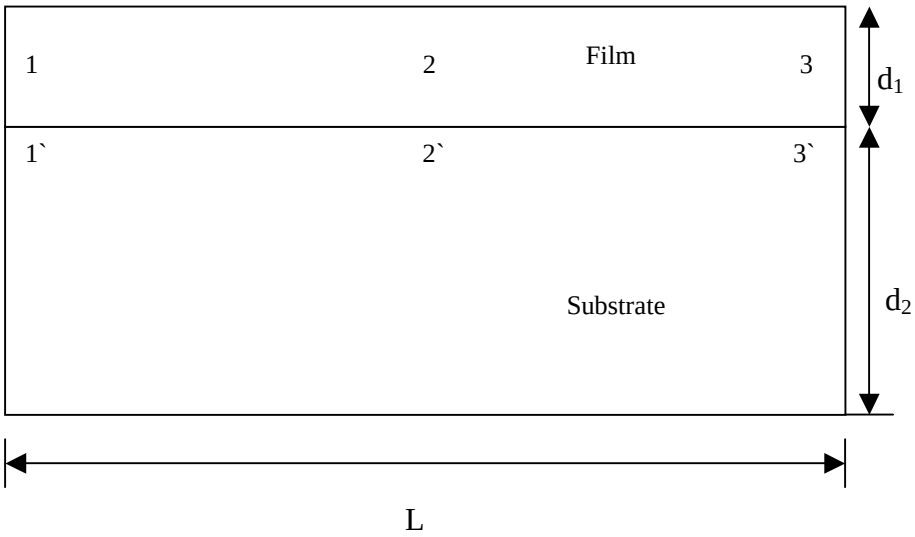

For d_1 = 0.025 mm & d_2=1.5 mm, L = 50 mm

Location	Sxx(MPa)	Syy(MPa)	Location	Sxx(MPa)	Syy(MPa)
1	-588.45	-13.058	1`	73.401	-21.01
2	-630.02	0	2`	42.482	0
3	-588.45	-13.058	3`	73.401	-21.01

For d_1 = 0.010 mm & d_2 = 1.5 mm, L = 50 mm

Location	Sxx(MPa)	Syy(MPa)	Location	Sxx(MPa)	Syy(MPa)
1	-660.63	0	1`	17.7	0
2	-660.63	0	2`	17.702	0
3	-660.63	0	3`	17.7	0

The calculations show that the film is biaxial compression. Thus, it is not expected to crack. However, there is potential for delamination, and it should increase with increasing film thickness. This aspect will be discussed in later reports.

Synthesis of Nanosize YSZ Powders: The electrocatalytic activity of composite electrodes critically depends on the electrode microstructure; in particular the size of the electrolyte component of the electrode. Since YSZ is the constituent in both electrodes, it is imperative that it should be as fine as possible. An effort was thus initiated to develop a process for the synthesis of nanosize powder. A manuscript based on this work is ready for submission to a refereed journal for publication. A copy of this manuscript is attached as part of this report.

Finite Element Analysis of Film and Substrate

Finite element analysis of following film (YSZ electrolyte) - substrate (Ni + YSZ anode) was performed by using ANSYS 5.5 (Finite Element Analysis package). The analysis is steady state structural analysis and the element used is PLANE42.
Following parameters were used in the analysis:
α_1 = Coefficient of thermal expansion of the film. =10.5 x 10^{-6} /^{o}C
α_2 = Coefficient of thermal expansion for substrate. =13 x 10^{-6}/°C
E_1 = Young's modules of elasticity for film = 210 GPa
E_2 = Modules of Elasticity for substrate. = 170 GPa
$\Delta\varepsilon = \Delta\alpha\Delta T$=3.25 x 10^{-3}

Coordinate System:

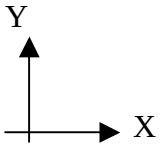

Figure 1:

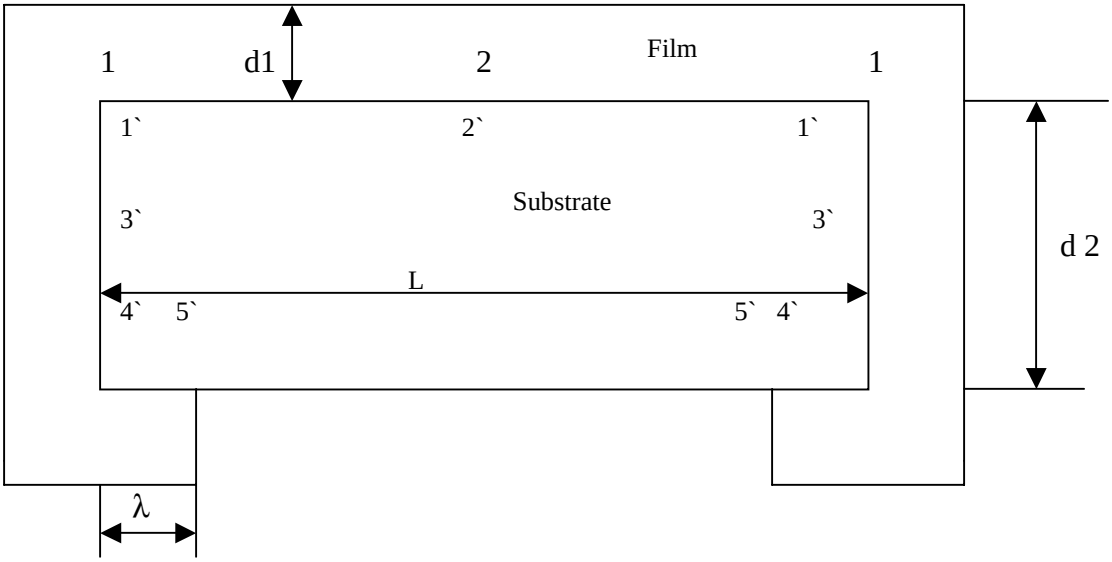

λ = 5 mm, d_1 = 0.025 mm, d_2 = 1.5 mm, L = 50 mm.

Location	Sxx(MPa)	Syy(MPa)	Location	Sxx(MPa)	Syy(MPa)
1	-207.98	-409.00	1`	59.085	56.458
2	-606.37	-0.43E-03	2`	61.627	-0.88E-03
3	-0.788	-656.58	3`	-1.026	61.383
4	-431.04	-172.26	4`	60.205	65.515
5	-620.73	8.781	5`	-0.57E-01	2.73

Figure 2:

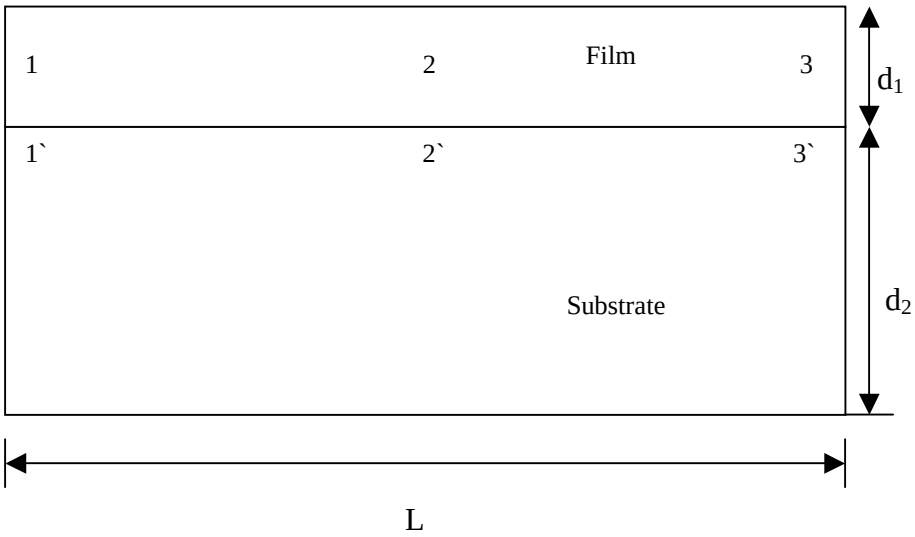

For d_1 = 0.025 mm & d_2=1.5 mm, L = 50 mm

Location	Sxx(MPa)	Syy(MPa)	Location	Sxx(MPa)	Syy(MPa)
1	-588.45	-13.058	1`	73.401	-21.01
2	-630.02	0	2`	42.482	0
3	-588.45	-13.058	3`	73.401	-21.01

For d_1 = 0.010 mm & d_2 = 1.5 mm, L = 50 mm

Location	Sxx(MPa)	Syy(MPa)	Location	Sxx(MPa)	Syy(MPa)
1	-660.63	0	1`	17.7	0
2	-660.63	0	2`	17.702	0
3	-660.63	0	3`	17.7	0

The calculations show that the film is biaxial compression. Thus, it is not expected to crack. However, there is potential for delamination, and it should increase with increasing film thickness. This aspect will be discussed in later reports.

SYNTHESIS OF NANOSIZE YTTRIA-STABILIZED ZIRCONIA BY A MOLECULAR DECOMPOSITION PROCESS

Yi Jiang, Sanjeevani V. Bhide and Anil V. Virkar[1]

Department of Materials Science and Engineering, 122 South Central Campus Drive, Rm 304, University of Utah, Salt Lake City, Utah 84112

ABSTRACT

Nanosize yttria-stabilized zirconia (YSZ) was synthesized by a unique approach based on molecular decomposition. In this approach, yttria-doped $BaZrO_3$ (Y-$BaZrO_3$) or yttria-doped Na_2ZrO_3 (Y-Na_2ZrO_3) precursors were first synthesized from $BaCO_3$, ZrO_2, Y_2O_3 or $BaCO_3$ and commercial YSZ for Y-$BaZrO_3$, and from Na_2CO_3 and YSZ for Y-Na_2ZrO_3, by a conventional solid state reaction method. Then, the precursors were boiled to leach away the unwanted species, BaO or Na_2O, either in a dilute HNO_3 soultion in water in the case of Y-$BaZrO_3$, or in de-ionized water in the case of Y-Na_2ZrO_3. During boiling in HNO_3 or water, the insoluble residue of Zr-Y-O composition formed fine, nanosize YSZ particles. X-ray diffraction (XRD) and specific surface area measurements on the as-synthesized powders confirmed the formation of nanosize YSZ. A subsequent heating in air led to particle growth. However, for a treatment at a temperature as high as 1000^{o}C, the particle size was well in the nanosize range. XRD showed that the as-synthesized YSZ powders, as well as those heated up to 1000^{o}C, the maximum temperature the powders were heated to after leaching, are of cubic structure.

I. INTRODUCTION

Nanosize powders have numerous applications such as catalysts, photo-catalysts, electro-catalysts, catalyst supports [1], electrodes, active powders for the fabrication of dense bodies [2], semiconductors for energy storage, photovoltaics [3], ultrafine magnetic materials for information storage [4], environmental clean-up as destructive adsorbents [5], water purification [6], and optical computers [7], to name a few. The synthesis of nanosize materials has received considerable attention over the past decade or so. Several processes have been developed and are currently being used for the synthesis of nanosize powders. These processes include (1) Gas-phase condensation, (2) Mechanical milling [8], (3) Thermal

[1] To whom all correspondence should be addressed.

crystallization, (4) Chemical precipitation [9], (5) Sol-gel process, (6) Aerosol spray pyrolysis [10], etc.

In gas-phase condensation, evaporation of precursors and their interaction with an inert gas leads to loss of kinetic energy, and homogeneous nucleation of nanosize powders occurs in a supersaturated vapor [11]. Nano-crystalline powders of TiO_2 [12], Li_2O-doped MgO [13], CeO_2 [14], Y-doped ZrO_2 [15], etc. have been produced by gas-phase condensation. Aerosol spray pyrolysis has been used to synthesize $BaFe_{12}O_{19}$ [16], Fe_2O_3 [17] among some other materials. High energy mechanical milling is used extensively to produce nanomaterials, especially when large quantities of materials are required. Very fine particles of nickel-aluminum alloys [18], Fe-Co-Ni-Si alloys [19], Ni-Mo alloys [20], for example, have been produced by mechanical milling. Contamination by the milling process, however, is a shortcoming of this process. Also, although very fine particles can be made, agglomeration is a problem leading to cluster sizes in the micron range.

Chemical co-precipitation has been studied extensively for the synthesis of nanosize powders [9]. Metallic as well as ceramic powders can be made by a careful control of chemistry. Alkali metal borohydride, MBH_4 where M is an alkali metal, for example, has been used as a reducing agent in aqueous media for the synthesis of metallic powders. It is important to control the pH and the ionic strength in aqueous media to prevent Ostwald ripening [9]. In the synthesis of nanosize iron oxide, for example, it has been shown that the higher the pH and the higher the ionic strength, the smaller is the size of nanosize particles.

In this communication, we report a unique approach developed to synthesize nanosize yttria-stabilized zirconia (YSZ) powder. There are many reports in the literature on the synthesis of nanosize YSZ powders by processes such as sol-gel process [21], inert gas condensation [22], plasma technique [23], chemical co-precipitation [24] and aerosol combustion [25], etc. All of these methods are based on molecular synthesis of nanoparticles wherein the particles are built-up by an atom by atom or by a molecule by molecule addition. Thus, the growth of particles inevitably occurs during the process itself. In order to ensure the formation of nanosize powders, in such processes a careful control over nucleation and growth is required.

The approach we report in this paper is based on molecular decomposition, rather than molecular synthesis, in which, a precursor powder (either of a micro or macro size, containing the desired elements) is first synthesized by a conventional method, such as a high temperature solid state reaction. Then, the unwanted species are chemically leached away in a suitable liquid; which may be just water, or a dilute acid solution [26]. During the leaching process, the concomittant change in volume and crystal evolution leads to the formation of very fine (molecular level) fragments, thus leading to the formation of nanosize powders. Since neither the precursor nor the product is soluble in the selected liquid, growth of particles can not occur, since the latter necessarily requires the occurrence of dissolution-reprecipitation. Therefore, particle coarsening can be successfully prevented. This approach is also ideally suited for the commercial production of nanosize powders since the process does neither require exotic equipment nor exotic processes. In the present communication, 8 mol.% yttria-stabilized zirconia (YSZ) nanosize powder was successfully prepared by this approach using two different precursors, 8 mol.% yttria-doped Na_2ZrO_3 (Y-Na_2ZrO_3) and 8 mol.% yttria-doped $BaZrO_3$ (Y-$BaZrO_3$). In the case of Y-Na_2ZrO_3, the liquid used was water. In the case of Y-$BaZrO_3$, the liquid used was dilute nitric acid. The synthesized powders using either precursor were nanosize, as-determined by XRD and specific surface area measurement. Also, it was determined by XRD that the as-synthesized powders are of cubic structure, as expected for 8 mol.% YSZ. The powders retained the cubic structure to 1000^oC, the maximum temperature to which the powders were heated after synthesis.

II. EXPERIMENTAL PROCEDURE

For the synthesis of nanosize yttria-stabilized zirconia, the precursor can be a suitable alkali or alkaline earth zirconate. Two types of precursors, i.e. yttria-doped barium zirconate, (Y-$BaZrO_3$), and yttria-doped sodium zirconate, (Y-Na_2ZrO_3), were synthesized by a conventional solid state reaction method. For preparing Y-$BaZrO_3$, the starting materials, namely, $BaCO_3$, ZrO_2 and Y_2O_3, or $BaCO_3$ and a commercial yttria-stabilized zirconia (YSZ) powder, were mixed in requisite proportions, wet ball-milled in alcohol for 24 h and then dried. For the synthesis of Y-Na_2ZrO_3, Na_2CO_3 and commercial YSZ powder were mixed in a requisite proportion, wet ball-milled and then dried. The ball-milled and dried powder mixtures were calcined at various temperatures and the resulting powders were examined by x-ray diffraction (XRD) with Cu$K\alpha$

radiation to identify calcination conditions which ensure the formation of completely converted, single phase, precursor powders; i.e., Y-$BaZrO_3$ or Y-Na_2ZrO_3.

Doped sodium zirconate was then boiled and washed in de-ionized water since the reaction between Na_2ZrO_3 and water is thermodynamically favored. In this way, Na_2O can be easily leached out. To ensure the complete removal of Na_2O, the powder was continuously washed until the pH of the solution was near neutral (~7). Then, the resulting powder was dried and later characterized. The Gibbs free energy change for the reaction of barium zirconate with water at or near room temperature is close to zero [27] indicating that $BaZrO_3$ is thermodynamically stable in the presence of water. Thus, water is not a suitable leaching agent for $BaZrO_3$. A dilute acid solution is necessary to facilitate the removal of BaO from barium zirconate. Y-doped barium zirconate was boiled in dilute HNO_3 acid (0.07M) repeatedly until no further change in the pH of the solution occurred. Then, the powder was thoroughly washed with de-ionized water and dried.

Differential Thermal Analysis (DTA) was conducted to examine the as-synthesized powders. In the DTA experiments, the samples were purged with purified air and heated up to 1200^{o}C at a heating rate of 10^{o}C/min. Based on the DTA information, several temperatures were identified for the calcination of the powders after the leaching treatments. The calcined powders were then examined by XRD.

III. RESULTS AND DISCUSSION

Figure 1 shows the XRD traces of Y-$BaZrO_3$ powders made from the calcination of $BaCO_3$, ZrO_2 and Y_2O_3, and from $BaCO_3$ with YSZ, at 1250^{o}C for 2h. The traces are almost identical and match the standard trace for the cubic structure of perovskite, $BaZrO_3$. There are no other additional peaks present, indicating that the solid state reaction was complete resulting in the formation of a single phase, Y_2O_3-doped $BaZrO_3$. The results also show that yttria-doped $BaZrO_3$ can be synthesized with either of the starting materials at a temperature of 1250^{o}C or above. Figure 2 is an XRD trace of the Na_2CO_3 and YSZ mixture after calcining at 1250 ^{o}C for 2h, which corresponds to monoclinic sodium zirconate, Na_2ZrO_3. Since YSZ was used instead of ZrO_2, it is expected that Na_2ZrO_3 formed should be yttria-doped, i.e., Y-Na_2ZO_3. Again, XRD

revealed that the reaction was complete with only one phase formed. A calcination temperature lower than 1050^{o}C was not high enough to ensure the completion of the reaction, as evidenced by the lack of formation of a single phase material.

Chemical leaching of BaO from yttria-doped $BaZrO_3$ (Y-$BaZrO_3$) precursor was achieved using a dilute HNO_3 solution in water. The precursor was boiled in a dilute HNO_3 acid solution, filtered and washed repeatedly until the solution pH was unchanged. Then, it was thoroughly washed using de-ionized water to completely remove Ba as $Ba(NO_3)_2$. The solution containing the leachable ions was chemically analyzed to determine the concentrations of Ba, Y, and Zr. The results showed (Table 2) a significant concentration of Ba^{2+} but only trace concentrations of Zr^{4+} and Y^{3+}, confirming that Ba^{2+} was selectively dissolved and led to the formation Y_2O_3-ZrO_2, which is insoluble in the dilute HNO_3 solution, by a reaction such as

$$Y\text{-}BaZrO_3 + 2HNO_3 \rightarrow Ba(NO_3)_2 + Y_2O_3\text{-}ZrO_2 \quad (1)$$

For the yttria-doped doped Na_2ZrO_3 (Y-Na_2ZrO_3) precursor, since Na_2ZrO_3 readily reacts with water by a reaction such as

$$Na_2ZrO_3 + 2H_2O \rightarrow 2NaOH + Y_2O_3\text{-}ZrO_2 \quad (2)$$

repeated boiling in de-ionized water, filtering and washing was adequate to completely remove Na_2O as NaOH. In this case also, the chemical analysis showed that the solution contained predominantly Na, but only trace amounts of Y and Zr (Table 3). XRD traces of leached and washed powders synthesized from the two precursors are given in Figure 3(a). In both cases, XRD traces of leached and washed powders were quite different from those of the corresponding precursors (Y-Na_2ZrO_3 and Y-$BaZrO_3$). At the same time, the XRD traces of the leached and washed powders were identical, regardless of the precursor, Y-Na_2ZrO_3 or Y-$BaZrO_3$. Figure 3(b) shows an XRD trace of commercial YSZ. It is readily seen that the XRD traces of the leached and washed powders are similar to the commercial YSZ, insofar as peak positions are concerned. This shows that during leaching of the respective precursors, only BaO or Na_2O is leached away resulting in a residue containing Y, Zr, and O such that the Zr-Y-O skeleton has a cubic symmetry. The XRD peaks in the traces of leached powders, however, are very broad indicative of a very fine particle size. This shows that very fine (nanosize) particles of YSZ can be formed starting with precursors (Y-$BaZrO_3$ or Y-Na_2ZrO_3) whose particle size is several microns.

The formation of nanosize powders, starting with coarse precursor powders, can be illustrated via the following example. Let us consider the reaction of Y-$BaZrO_3$ with dilute HNO_3. The precursor, Y-$BaZrO_3$ is insoluble in dilute HNO_3. However, it can react with HNO_3, as given by equation (1). The volume of a Y-$BaZrO_3$ unit cell is about 73.72 A^3. One unit cell of cubic zirconia contains four formula units, i.e. 4 'ZrO_2' or 4 'Y-ZrO_2', with a volume of 135.72 A^3. Thus, per one formula unit, such as is created per one Y-$BaZrO_3$ unit cell, the volume is 135.72/4 or 33.93 A^3. Thus, as Y-$BaZrO_3$ reacts with HNO_3 to form Y-ZrO_2, there is a net change in volume from 73.72 A^3 to 33.93 A^3. This is equivalent to $\frac{(73.72-33.93)}{73.72}\times 100 \approx 54\%$ decrease in volume. In terms of a linear change, this corresponds to $\frac{\sqrt[3]{73.72}-\sqrt[3]{33.93}}{\sqrt[3]{73.72}}\times 100 \approx 25\%$ decrease in a linear dimension. As the surface of the precursor particle reacts with HNO_3 to form soluble $Ba(NO_3)_2$, there is a substantial volume change and a linear change (a decrease), which should lead to cracks and fissures at the unit cell (A) level. This should thus lead to the formation of tiny fragments at the angstrom or nanosize level. As the product, Y-ZrO_2 is insoluble (or has a very low solubility) in the liquid used, Ostwald ripening, which requires dissolution, transport and reprecipitation, should not occur. Figure 4 shows a schematic of the leaching process of Y-$BaZrO_3$ in dilute HNO_3. The outer layer of the particle is porous since BaO (as $Ba(NO_3)_2$) is leached out of Y-$BaZrO_3$. Further reaction occurs by the transport of HNO_3 to the porous YSZ/dense Y-$BaZrO_3$ interface, reaction to form $Ba(NO_3)_2$ and YSZ, and the transport of dissolved $Ba(NO_3)_2$ away from the interface, through the porous YSZ, into the acid bath. The porous YSZ is easily fragmented into very fine powder. Thus, even though the original Y-$BaZrO_3$ powder is coarse, the resulting YSZ powder should be nanosize. This is the origin of this process for the synthesis of nanosize powders. The preceding also suggests that the initial precursor particle size should have no bearing on the final size of nanoparticles. Indeed, nanosize powder can be synthesized using precursors that are considerably coarse; for example in the micron size range.

The Scherrer formula relates the average particle size, *d*, to X-ray peak broadening, *B*, by

$$d = \frac{0.9\lambda}{B\cos\theta} \qquad (3)$$

In order to determine the peak broadening attributable only to the particle size effect, a commercial YSZ powder was sintered at 1500^{o}C for a few hours to obtain a strain-free, coarse-grained (grain size on the order of a few microns) sample. An XRD trace of the sample was obtained. Peak width (at half the peak height) from this sample for a given (*hkl*), in the present case (111), was subtracted from the corresponding peak width of the leached and washed powders. In this manner, line broadening attributable to the instrument as well as the presence of both $K\alpha_1$ and $K\alpha_2$, could be corrected for. The corrected peak width was measured to be approximately 4^{o} (~0.07 radians) for the case of washed powders, which is equivalent to an average particle size of about a few nanometers for both washed powders (Table 1).

As an independent confirmation of the nanosize of the powders formed, specific surface area measurements were conducted using the BET adsorption isotherm method. The surface area measurements were made on both the precursors (Y-Na_2ZrO_3 and Y-$BaZrO_3$) and the synthesized powders. The specific surface area of the precursors was typically only ~3 m^2/g (Table 4), consistent with the large particle size of the precursors. The specific surface area of the naonosize powder made from the Na_2ZrO_3 precursor, however, was measured to be around 67 m^2/g. Assuming particles to be spherical in shape for simplcity, the diameter of the particle can be estimated from the relation

$$d = \frac{6}{S\rho} \qquad (4)$$

where ρ is the density of YSZ and S is the specific surface area. Assuming ρ = 5.9 g/cm^3 for YSZ and 70 m^2/g for S, the diameter is estimated around 15 nm, which is in reasonably good agreement with the value estimated from XRD peak broadening measurements.

> The above results conclusively demonstrate that nanosize YSZ powder can be effectively prepared by this molecular decomposition approach using alkali or alkaline earth metal oxide precursors. Although the preparation was carried out at low temperature (near room temperature), cubic crystal structure YSZ was formed.

In order to examine the possible changes in the crystal structure of the synthesized nanosize YSZ powders, Differential Thermal Analysis (DTA) on the as-washed powders was conducted. In

addition, XRD traces were obtained on powders after heat treating the as-washed powders at various temperatures. Figure 5 shows the DTA curves of YSZ nanopowders synthesized from both precursors. The peaks centered around 235^{o}C in both traces are attributed to the endothermic desorption of adsorbed water. The traces also show broad exothermic peaks in the temperature range of 300–600^{o}C. An exothermic peak is usually attributed to the crystallization process, provided as-formed powders are amorphous. In the present case, the as-synthesized powder is crystalline – not amorphous, unlike some DTA data from YSZ precursors prepared by sol-gel or chemical co-precipitation. In such cases, the exothermic peak, i.e. the crystallization peak, is generally well-defined and sharp [21]. In the present work, by contrast, the exothermic peak is very broad for powders made using either of the precursors, but more so in the case of nanosize YSZ powder made from Y-$BaZrO_3$ precursor, indicating that there is neither the occurrence of a distinct crystallization, nor the occurrence of a phase transition over the temperature range investigated. The broad exothermic peak may be attributed to the possible removal of point defects, and/or the occurrence of particle growth during the thermal treatment. The occurrence of particle growth during thermal treatment can readily verified by XRD examination of nano YSZ powders pretreated at various temperatures.

Figure 6 shows the XRD spectra of nano YSZ powders thermally treated at various temperatures for 1.5 h. It can be seen that the crystal structure of the YSZ powder is unaffected by the thermal treatment, all the way up to 1000^{o}C, the maximum temperature to which the synthesized powders were heated. This, of course, is not surprising as the stable phase of 8 mol.% Y_2O_3-stabilized zirconia is known to be cubic over the entire temperature range of the existence of the solid phase. As the temperature of heat treatment is increased, the peak height increases at the expense of peak width, consistent with the occurrence of particle growth. The estimated particle size of the powders after heat treatment at 1000^{o}C is about 30 nm, showing that the nanosize particles are relatively stable against a significant growth at temperatures as high as 1000^{o}C. Heat treatment of nanosize YSZ obtained from Y-Na_2ZrO_3 precursor (Figure 7) leads to similar results.

Table 1 gives the average particle size of YSZ powders, treated at various temperatures after synthesis, calculated from the Scherrer formula using the half peak width from the XRD traces in

Figures 6 and 7. For the nanosize YSZ powder synthesized from Y-Na_2ZrO_3 precursor, the particle size is only a few nanometers until the heat treatment temperature is raised to 350^oC. A substantial particle growth occurred, however, at higher temperatures. The remarkable increase in particle size above 350^oC coincides with the peak in DTA centered around 350^oC. This shows that the broad exotherm observed in the DTA peaks may be associated with the growth of particles rather than crystallization. After a thermal treatment at 1000^oC for 5 h, the surface particle size as measured by XRD is still small, around 30 nm. The corresponding specific surface area measured was ~13.6 m^2/g. YSZ powder prepared from Y-$BaZrO_3$ also exhibits similar behavior. In the case of powder made with Y-$BaZrO_3$, the particle size exhibited substantial growth (to ~23 nm) after treatment at 650^oC. This observation is consistent with the occurrence of a broad exotherm in the corresponding DTA trace. The particle sizes of YSZ from both precursors are similar, which are in the range from a few nanometers to tens of nanometers after thermal treatment at a temperature as high as 1000^oC. An investigation of the sinterability of YSZ powders made by the present process, and the measurement of ionic conductivity of sintered samples is underway. The results of these studies will be reported in a separate communication.

IV. CONCLUSIONS

Nanosize YSZ powder was prepared by a unique approach, in which yttria-doped $BaZrO_3$ or yttria-doped Na_2ZrO_3 precursors were first synthesized by a solid state reaction. Then, then the unwanted species, BaO or Na_2O, was leached away by washing the precursors in a dilute HNO_3 solution or in water. This led to the formation of very fine, nanosize yttria-stabilized zirconia (YSZ). The particle size of the as-syntheszied YSZ powders was a few nanometers and increased to tens of nanometers after thermal treatment at a temperature as high as 1000^oC. The as-synthesized as well as heat-treated YSZ powder was of cubic crystal structure.

Acknowledgments: This work was supported by the U. S. Department of Energy, NETL, Contract No. DE-AC26-99FT40713.

Table 1: Particle size (nm) of as-synthesized nanosize YSZ powder and after heating in air at various temperatures for 1.5 h.

Temperature (^oC)	YSZ from Y-$BaZrO_3$ *d* in nm	Temperature (^oC)	YSZ from Y-Na_2ZrO_3 *d* in nm
as washed	2.4	As-washed	2.4
350	8.0	300	4.8
450	10	350	17
650	23	650	18
1000*	37	1000*	31

*for 5 hours

Table 2: Chemical analysis of the leaching solution (dilute HNO_3) after boiling Y-$BaZrO_3$ in it.

Powder	Solution	Barium (mol/l)	Yttrium (mol/l)	Zirconium (mol/l)
Y:$BaZrO_3$	0.3 M HNO_3	0.104	$7.11x10^{-4}$	$< 2.0x10^{-5}$
Y:$BaZrO_3$	0.07 M HNO_3	0.062	$3.0x10^{-5}$	$< 2.0x10^{-5}$

Table 3: Chemical analysis of the leaching solution (water) after boiling Y-Na_2ZrO_3 in it.

Powder	***Sodium*** (mol/l)	***Yttrium*** (mol/l)	***Zirconium*** (mol/l)
Y:Na_2ZrO_3	***0.713***	***$< 5 x 10^{-5}$***	***$< 5 x 10^{-5}$***

Table 4: Surface areas of as-calcined precursors, as-synthesized nanosize YSZ, and after hetaing the nanosize YSZ to 1000^{o}C for 5 hrs.

Sample	Y-$BaZrO_3$	Y-Na_2ZrO_3	As-synthesized Nanosize YSZ	Nanosize YSZ after 5 hrs. at 1000^{o}C
Surface Area (m^2/g)	3.5	2.7	66.6	13.6

REFERENCES

1) J.Y. Ying, in '*Nanophase Materials: Synthesis – Properties – Applications*', edited by G. C. Hadjipanayis and R. W. Seigel, NATO ASI Series E: Applied Sciences – Vol. 260, p.37-44, Kluwer Academic Publishers (1994)
2) G. Skandan, *NanoStructured Materials*, **5** [2] 111-126 (1995).
3) L. V. Interrante and M. J. Hampden-Smith, 'Chemistry of Advanced Materials: An Overview', Wiley-VCH (1998).
4) M. L. Trudeau and J. Y. Ying, *NanoStructured Materials*, **7** [1-2] 245-258 (1996).
5) Y. X. Li, O. Koper, M. Atteya and K. J. Klabunde, *Chem. Materials*, **4** 323-330 (1992).
6) T. Boronia, K. J. Kalbunde and G. B. Sergeev, *Environ. Sci. Technol.*, **29** 1511-1517 (1995).
7) N. Herron, *Chem. Technol*., **19** 542-548 (1989).
8) H. J. Fecht, in '*NANOMATERIALS: Synthesis, Properties and Applications*' edited by A. S. Edelstein and R. C. Cammarata, Institute of Physics Publishing, Bristol and Philidelphia, p.89-110 (1996).
9) K. J. Klabunde, J. V. Stark, O. Koper, C. Mohs, A. Khaleel, G. Glavee, D. Zhang, C. M. Sorensen and G. Hadjipanayis, in Ref. (1), p.1-19 (1994).
10) C. M. Sorensen, Q. Li, H. K. Xu, Z. X. Tang, K. J. Klabunde and G. C. Hadjipanayis, p.109-116 in Ref. (1), (1994).
11) H. Gleiter in '*Deformation of Polycrystals: Mechanism and Microstructures*', edited by N. Hansen, A. Horsewell, T. Leffers and H. Lilholt, Riso National Laboratory, Rackilde, Denmark, p.15 (1981).
12) D. D. Beck and R. W. Siegel, *J. Mater. Res*., **7** 2840-2845 (1992).
13) H. W. Sarkas, S. T. Arnold, J. H. Hendricks, L. H. Kidder, C. A. Jones and H. K. Bowen, *Z. Phys. D*, **26** 46-50 (1993).
14) A. S. Tschope and J. Y. Ying, *NanoStructured Materials*, **4** 617 (1994).
15) A. Rouanet, G. Pichelin, C. Roucau, E. Snoeck and C. Monty, p.85-88 I Ref. (1), (1994).
16) Z. X. Tang, S. Nafis, C. M. Sorensen, G. C. Hadjipanayis and K. J. Klabunde, *IEEE Trans. Mag*., **25** 4236-4238 (1989).
17) Z. X. Tang, S. Nafis, C. M. Sorensen, G. C. Hadjipanayis and K. J. Klabunde, *J. Mag. Mater.*, **80** 285-289 (1989).
18) T. Benameur, R. Yavari and R. Durand, *Mater. Sci. & Eng.*, **A181/A182** 1145-1149 (1994).
19) M. L. Trudeau, J. Y. Huot, R. Schultz, D. Dussault, A. Van Neste and G. L'Espe'rance, *Phys. Rev. B*, **45** 4626-4636 (1992).
20) D. E. Brown, M. N. Mahmood, A. K. Turner, S. M. Hall and P. O. Fogarty, *Int. J. Hydrogen Energy*, **7** 405 (1982).
21) T. Okubo and H. Nagamoto, *J. Mater. Sci*., **30**, 749-757 (1995).
22) P. Mondal and H. Hahn, *Ber. Bunsen-Ges.* **101(11)**, 1765-1768 (1997).
23) J. Grabis, A. Ruzjukevics, D. Rasmane, M. Mogensen, S. Linderoth, *J. Mater. Sci*., **33** [3] 723-728 (1998).
24) T. L. Wen, V. Herbert, S. Vilminot, J. C. Bernier, *J. Mater. Sci*., **26**, 5184-5188 (1991).
25) J. Joseph, *J. Aerosol Sci*., **29** [5/6], 721-736 (1998).
26) 'A. V. Virkar and S. V. Bhide, 'A Molecular Decomposition for the Synthesis of Naonosize Powders', patent application filed, December 1998.
27) I. Barin, '*Thermochemical Data of Pure Substances*', 3rd. ed. Weinheim,New York, (1995).

FIGURE CAPTIONS

Figure 1: (a) An XRD trace of yttria-doped $BaZrO_3$ powder synthesized by calcining a mixture of $BaCO_3$, ZrO_2 and Y_2O_3 at 1250^oC for 2h. (b) An XRD trace of yttria-doped $BaZrO_3$ powder synthesized by calcining a mixture of $BaCO_3$ and YSZ at 1250 ^oC for 2 h.

Figure 2: An XRD trace of yttria-doped Na_2ZrO_3 powder synthesized by calcining a mixture of Na_2CO_3 and YSZ at 1250^oC for 2h.

Figure 3: (a) XRD traces of the residue after boiling Y-$BaZrO_3$ in dilute HNO_3 (Ba completely leached), and washing in water, and of the residue after boiling Y-Na_2ZrO_3 in de-ionized water (Na completely leached), and washing in water. (b) An XRD trace of a commercial YSZ powder.

Figure 4: A schematic showing a particle of Y-$BaZrO_3$ reacting with HNO_3. The porous outer layer is of YSZ. The dense inner region isI of the original Y-$BaZrO_3$. The reaction involves the following steps. (i) Transport of HNO_3 through the porous YSZ layer to the porous YSZ/dense Y-$BaZrO_3$ interface. (ii) Reaction between Y-$BaZrO_3$ and HNO_3 to form soluble $Ba(NO_3)_2$ and insoluble, porous YSZ. (iii) Transport of $Ba(NO_3)_2$ through the porous YSZ layer into the acid bath.

Figure 5: DTA traces obtained at 10^oC/min. in air, of nanosize YSZ powders synthesized from (a) Y-$BaZrO_3$ and (b) Y-Na_2ZrO_3 powders.

Figure 6: XRD traces of nanosize YSZ powders obtained from Y-$BaZrO_3$ subjected to subsequent thermal treatments at various temperatures.

Figure 7: XRD spectra of nanosize YSZ powders obtained from Y-Na_2ZrO_3 subjected to subsequent thermal treatments at various temperatures.

Figure 1

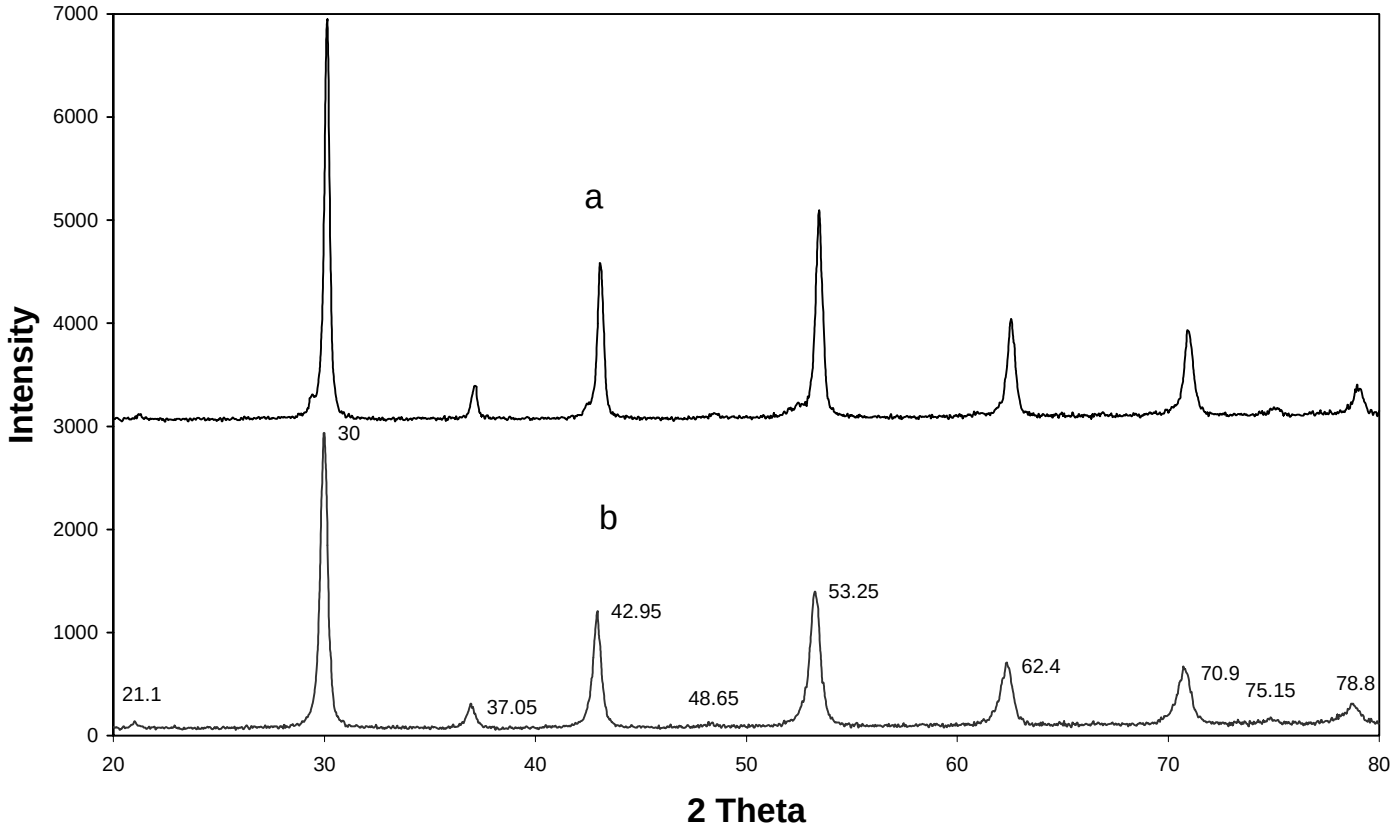
Intensity
2 Theta
a
b
30
21.1
37.05
42.95
48.65
53.25
62.4
70.9
75.15
78.8
0
1000
2000
3000
4000
5000
6000
7000
20
30
40
50
60
70
80

Figure 2

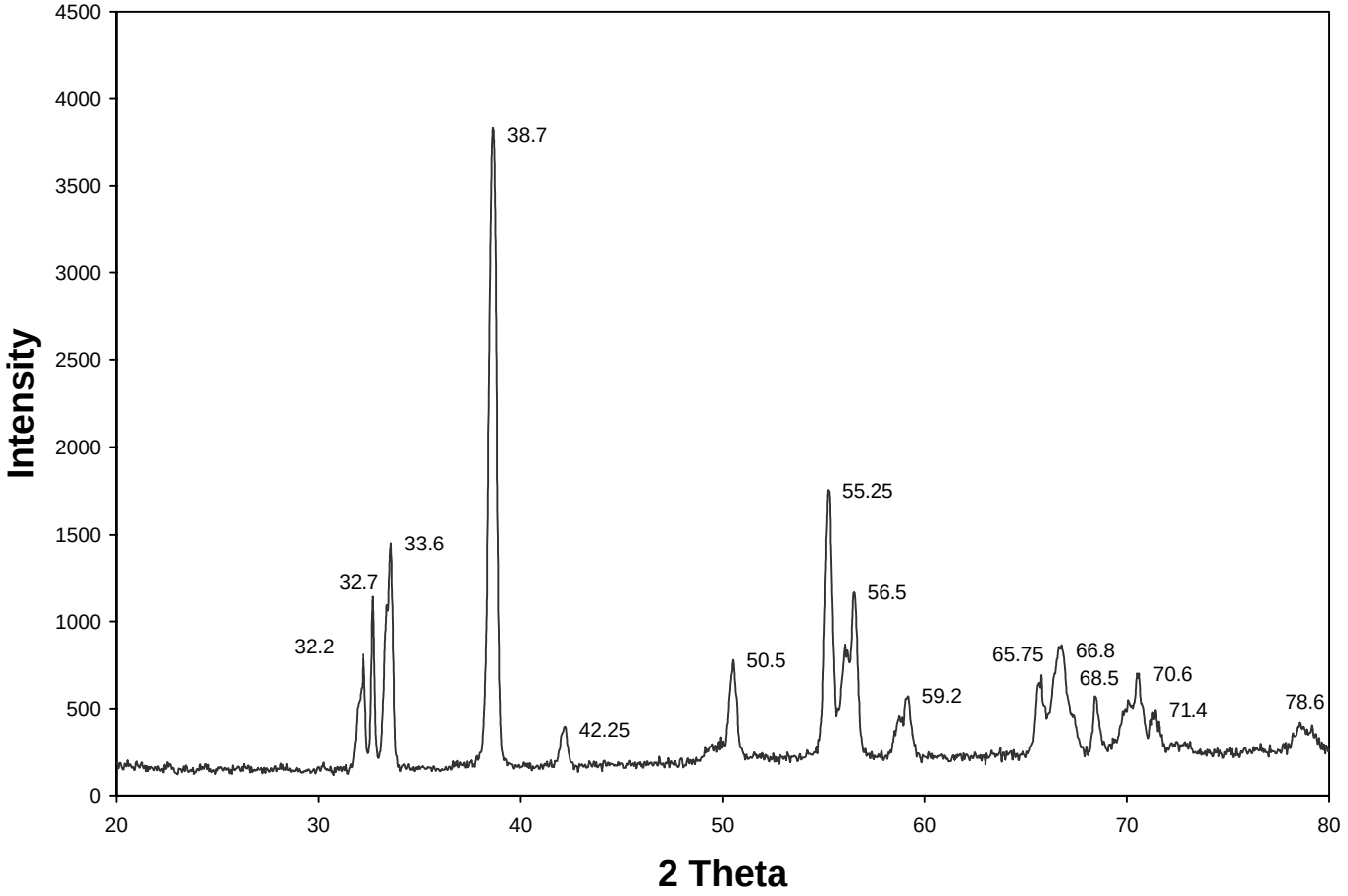
Intensity
2 Theta
4500
4000
3500
3000
2500
2000
1500
1000
500
0
20
30
40
50
60
70
80
38.7
32.2
32.7
33.6
42.25
50.5
55.25
56.5
59.2
65.75
66.8
68.5
70.6
71.4
78.6

Figure 3 (a)

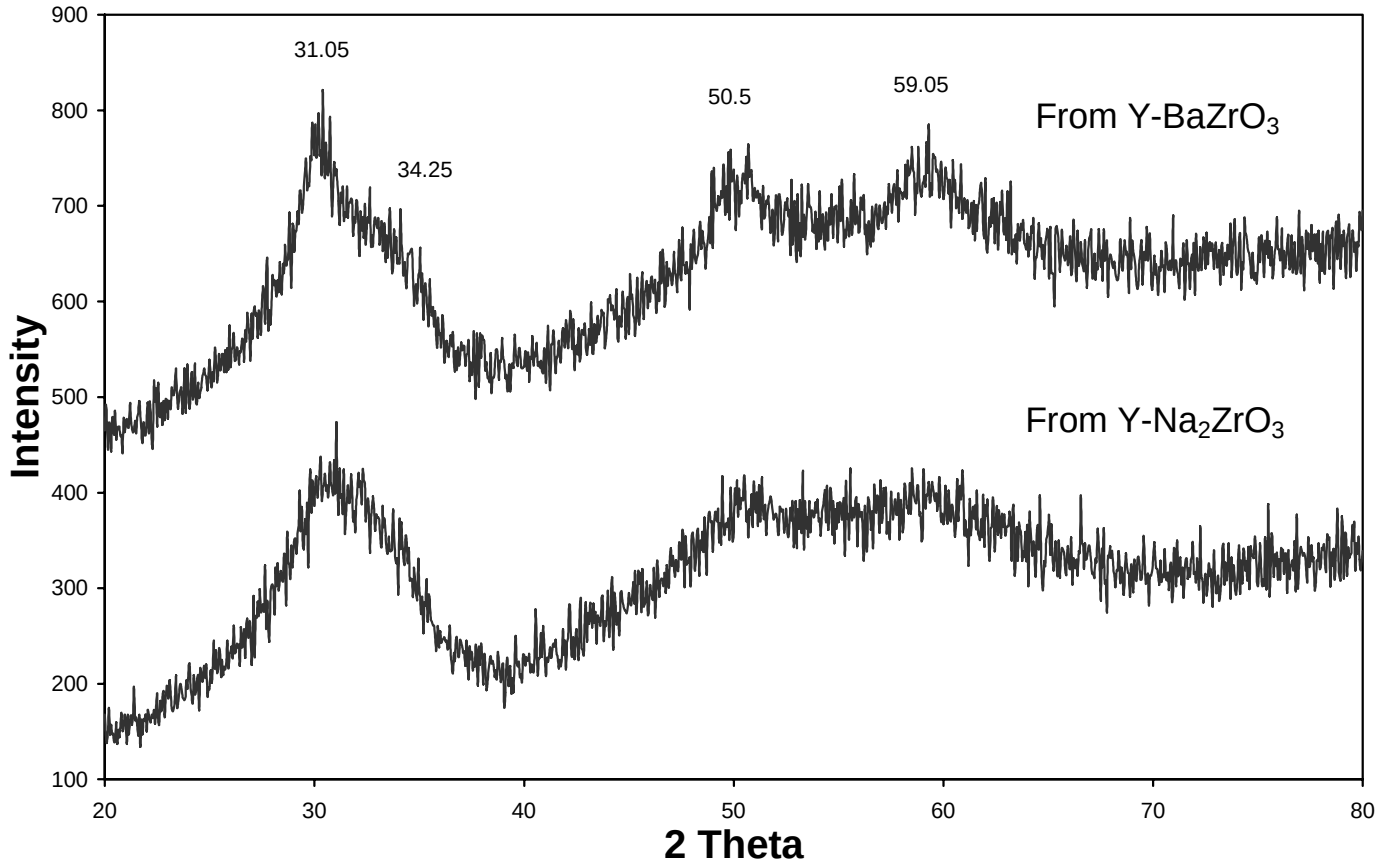
900
800
700
600
500
400
300
200
100
Intensity
20
30
40
50
60
70
80
2 Theta
31.05
34.25
50.5
59.05
From Y-BaZrO3
From Y-Na2ZrO3

Figure 3(b)

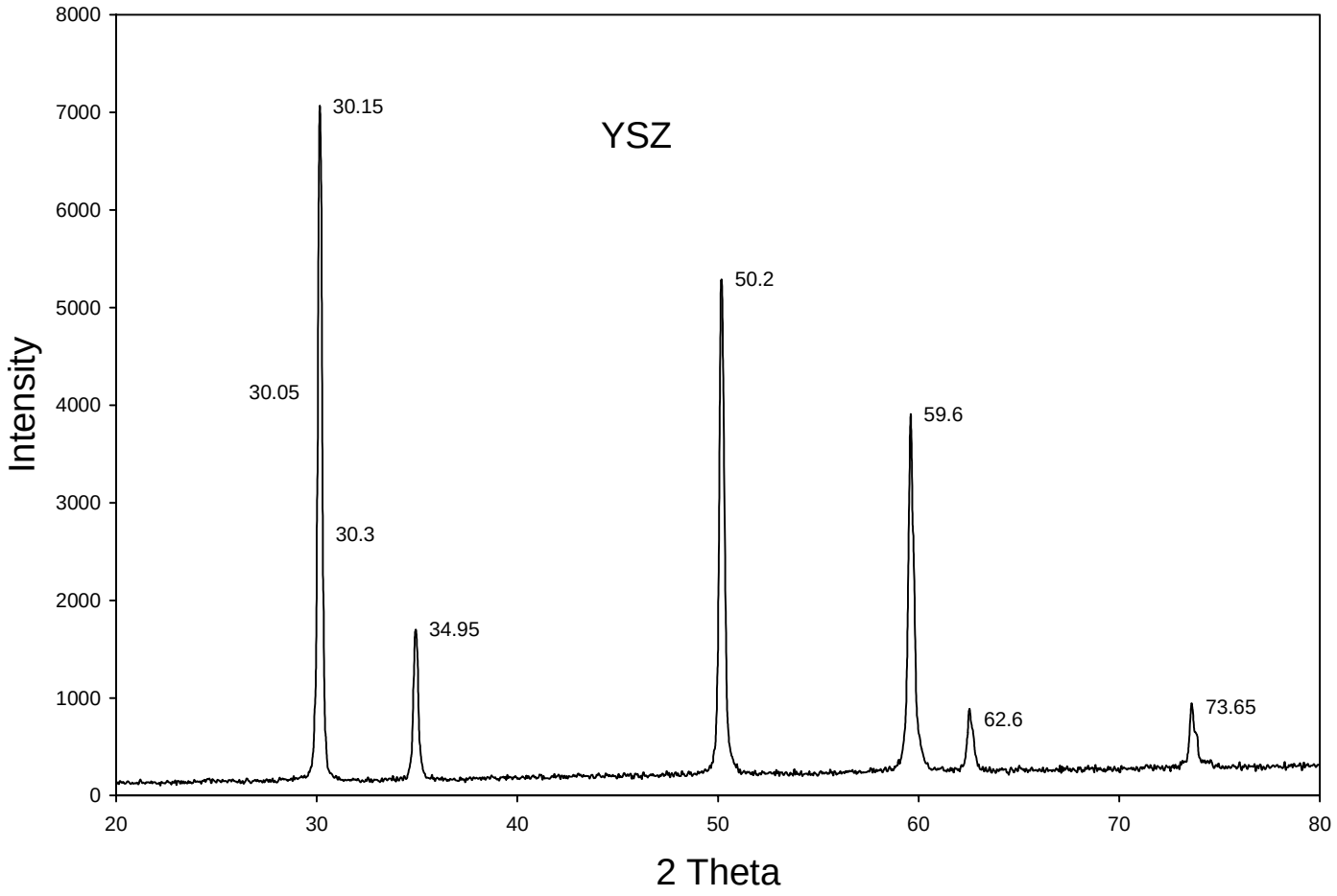
YSZ
Intensity
2 Theta
30.15
30.05
30.3
34.95
50.2
59.6
62.6
73.65
0
1000
2000
3000
4000
5000
6000
7000
8000
20
30
40
50
60
70
80

Figure 4

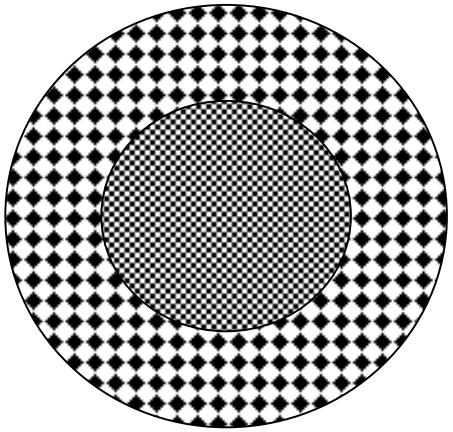

Original, Dense Y-$BaZrO_3$ Particle

Porous, Y-ZrO_2 (YSZ) after reaction with HNO3. $Ba(NO_3)_2$ is leached out.

Figure 5

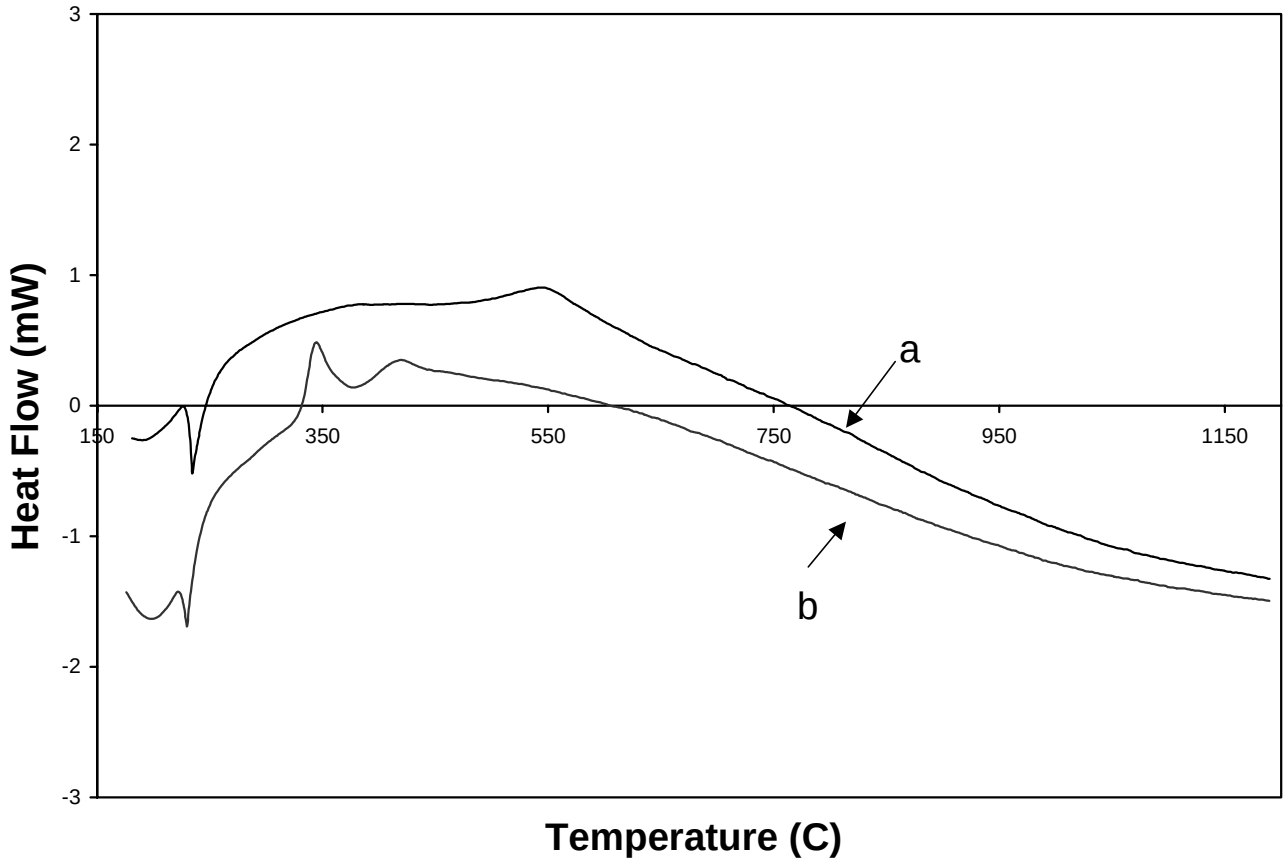
3
2
1
0
-1
-2
-3
150
350
550
750
950
1150
Heat Flow (mW)
Temperature (C)
a
b

Figure 6

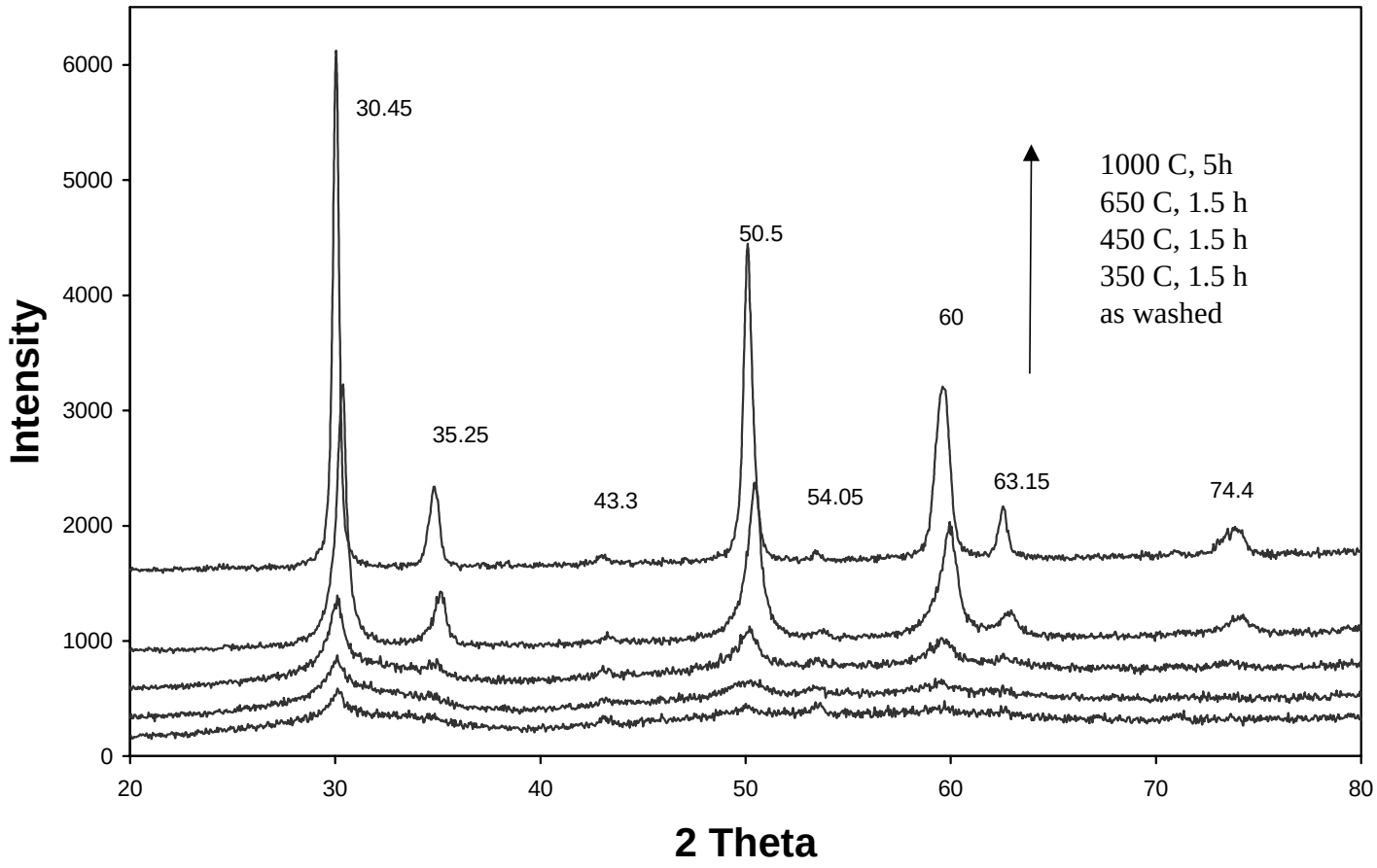
Intensity
2 Theta
30.45
35.25
43.3
50.5
54.05
60
63.15
74.4
1000 C, 5h
650 C, 1.5 h
450 C, 1.5 h
350 C, 1.5 h
as washed
0
1000
2000
3000
4000
5000
6000
20
30
40
50
60
70
80

Figure 7

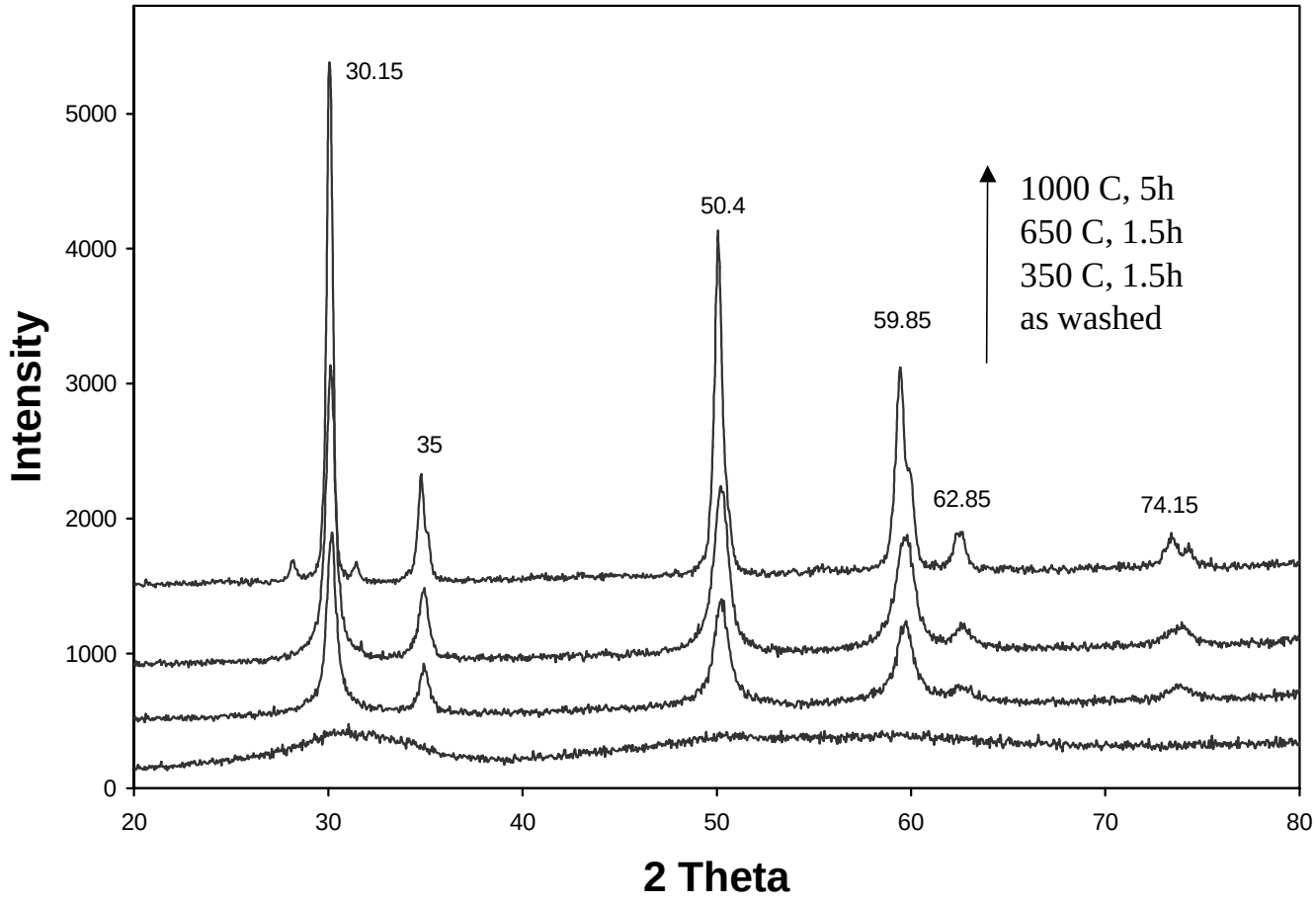
30.15
50.4
59.85
35
62.85
74.15
1000 C, 5h
650 C, 1.5h
350 C, 1.5h
as washed
Intensity
2 Theta
0
1000
2000
3000
4000
5000
20
30
40
50
60
70
80